Journal of Sound and Vibration (2001) **242**(5), 907–922
doi:10.1006/jsvi.2000.3397, available online at http://www.idealibrary.com on IDEAL®

CUTTING-INDUCED VIBRATION IN CIRCULAR SAWS

J. F. TIAN AND S. G. HUTTON

Department of Mechanical Engineering, University of British Columbia, Vancouver, B.C. Canada V6T 1Z4

(*Received* 30 *June* 1999, *and in final form* 2 *October* 2000)

An analytical model of a wood-cutting circular saw blade is developed for the purpose of understanding the mechanics of a lateral vibration instability known as washboarding. The governing equation developed contains inertial, gyroscopic and stiffness terms based upon the saw plate characteristics with the cutting forces being represented by the product of a time-dependent periodic function and the lateral displacement of the saw tooth. A stability analysis of the system is shown to produce predictions that are consistent with experimental data.

1. INTRODUCTION

A relatively common problem in the North American primary wood-cutting industry (i.e., that part of the industry involved with the production of sawn lumber from logs), is the appearance of a "washboard" pattern on the surface of the wood. Such a pattern is characterized by a sinusoidal-like variation in board thickness in both the cutting direction and normal to this direction. Figure 1 shows an example of such a pattern. (A related phenomenon occurs in metal cutting and is referred to as "chatter" in that context.) In the wood industry, the resulting board thickness variations are subsequently removed by the planing process. This results in higher than necessary sawdust production. The physical mechanisms that give rise to the washboarding phenomenon have not been clearly identified and the problem is dealt with in the industry by trial and error.

The general problem to be solved is that of predicting the self-excited vibrations that are involved in the interaction between a rotating flexible circular saw and a workpiece. The aim of the present work is to present an analysis of the stability characteristics of the blade while subjected to cutting forces and to define those circumstances under which washboarding will occur. A series of experimental studies [1] have been conducted in order to shed light on the mechanisms involved in the development of vibration dynamic instabilities that occur in wood-cutting saw blades.

Although much research has been conducted on circular saw dynamics in the past three decades, most of this research has focused on the dynamics of an idling saw blade. Carlin *et al.* [2] first studied the effects of a concentrated radial edge force on the natural frequencies of a spinning disc and analyzed the manner in which the asymmetric stress fields caused by the edge forces affect the natural frequencies of the disc. Radcliffe and Mote [3] considered a more general concentrated edge force with both radial and tangential components. Chen and Bogy [4] determined the membrane stress fields caused by a stationary friction force in a spinning disc, and found that these asymmetric membrane stress fields cannot cause instability in a spinning disc. Chonan *et al.* [5] studied the self-excited vibration of a pre-tensioned saw blade subjected to a small in-plane slicing force,

0022-460X/01/200907 + 16 $35.00/0

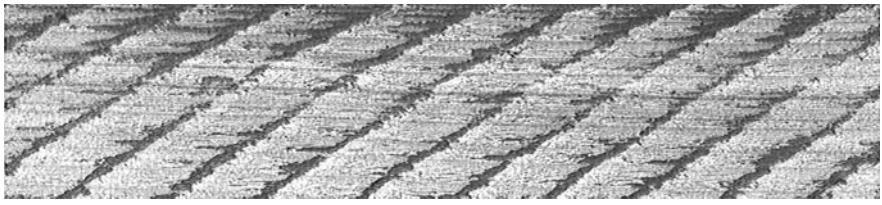

Figure 1. Washboarding pattern on a sawn board.

and their results also showed no significant effect of in-plane forces on the natural frequencies and stability of the blade.

Chen [6] reformulated the problem of a rotating disc subjected to a stationary concentrated in-plane radial force and included the effects of gyroscopic terms. It was reported in his paper that both divergence and flutter instabilities can be induced by stationary in-plane radial forces at critical or supercritical speeds. In an independent study, Shen and Song [7] treated a cutting saw blade as a rotating disc subjected to stationary follower edge forces with both radial and tangential components and predicted the instability of this system using the multiple scale method. It was reported in their paper that the radial edge force determines the rotating speed regions where the instability occurs and the tangential edge force only affects the width of the instability zones without introducing new unstable regions.

Recently Chen [8] modelled a saw-blade system as a spinning disc under a space fixed periodically varying edge force and investigated the dynamic stability of the rotating disc subject to a pulsating in-plane radial force by using an extended multiple scale method. Tian and Hutton [9] considered the stability analysis of a rotating disc subjected to a wide class of excitation mechanisms. The present study follows from this work and considers a cutting model involving multiple moving concentrated cutting forces over a given space-fixed sector to investigate the stability characteristics of the saw-blade and work-piece interaction. In previous research, the self-excited instability in saw-blade cutting was assumed to be produced by in-plane edge forces. A more important cutting force which was isolated in the experimental tests [1] conducted as a part of this study, and is the likely reason for the washboarding, has not been investigated in previous studies. This force is a lateral regenerative cutting force. Machine tool chatter in turning and milling operations is also induced by regenerative cutting forces. Machine tool chatter has been an active research topic for some time [10–14]. However, it appears that the work conducted in this field has not considered the gyroscopic effects associated with such systems [15].

New developments presented in this work involve solution methods for the stability analysis of a rotating disc subjected to multiple moving concentrated regenerative cutting forces over a given space-fixed sector. The basic Fourier series method is extended to solve the stability problem for time-varying equations with time-lag terms.

2. ANALYSIS OF INSTABILITIES DUE TO MULTIPLE MOVING REGENERATIVE CUTTING FORCES

In the dynamics of saw-blade cutting the cutting forces have traditionally been modelled as constant or pulsating in-plane edge forces [7, 6]. The force produced by flank cutting, which is likely to be the primary cause of the washboarding phenomenon, has been neglected in previous research. A detailed theoretical study on the instability induced in

a rotating saw by multiple moving regenerative cutting forces applied over a given space-fixed sector is presented in this section.

Figure 2 shows a diagrammatic representation of a rotating circular saw blade which cuts a work piece over a space-fixed sector. It can be seen from the sectional plot A–A that, if the blade oscillates laterally, there is an extra lateral cutting area between two successive teeth associated with both the transverse response $w(r_0, \theta_j, t)$ of the current tooth (the jth tooth) and the transverse response $w(r_0, \theta_j, t - T)$ of the previous tooth (the $(j-1)$th tooth) at a given location (r_0, θ_j) on the workpiece. T is the tooth-passing period (i.e., the period between successive tooth engagements). Lateral compression between the workpiece and the teeth in this extra cutting area causes the lateral cutting force $f_{cj}(t)$. This type of cutting force is called regenerative.

In actual cutting the saw blade will be subjected to radial and tangential in plane cutting forces as well as lateral forces. Exact modelling of such forces is difficult and is further complicated by the non-homogeneous nature of the wood. In this study, the following assumptions are made:

- The only forces acting are lateral forces caused by flank cutting.
- The cutting forces are always normal to the undeformed plane of the saw.
- The cutting forces are a linear function of relative tooth displacement.

Thus, the lateral regenerative cutting forces are assumed to be of the following linear form:

$$f_c(t) = \sum_{j=1}^{N_t} f_{cj}(t) = -\sum_{j=1}^{N_t} (1/r)K_r[w(r, \theta, t) - w(r, \theta, t - T)]\delta(r - r_0)\delta(\theta - \theta_j)g(\theta_j), \quad (1)$$

where N_t is the total number of saw teeth and K_r is a cutting force coefficient, assumed to be constant, which is determined by the geometry, properties and speeds of the blade, and by the characteristics of the workpiece. (For an anisotropic material, K_r would be a function of the position θ_j in the space-fixed co-ordinates.)

The deflection of the present and previous tooth at the location (r_0, θ_j) respectively are given by

$$w(r, \theta, t)\delta(r - r_0)\delta(\theta - \theta_j) = w(r_0, \theta_j, t)$$

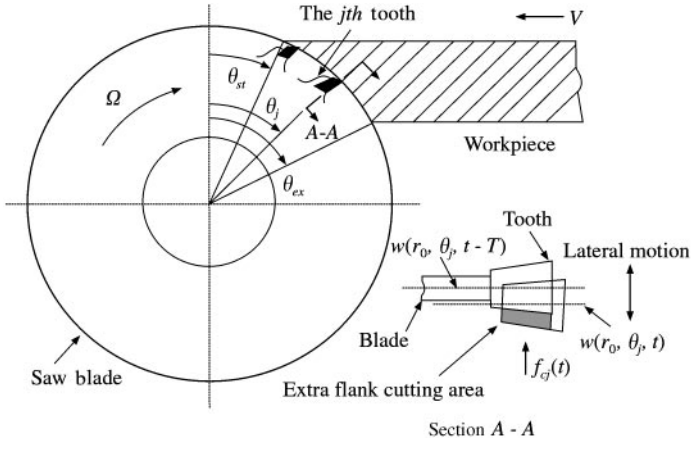

Figure 2. Lateral regenerative cutting force produced in a rotating circular saw.

and

$$w(r, \theta, t - T)\delta(r - r_0)\delta(\theta - \theta_j) = w(r_0, \theta_j, t - T),$$

where $T = 2\pi/(\Omega N_t)$, and

$$\theta_j = \theta_{st} + \Omega t + (j - 1)\theta_p \ (\theta_1 = \theta_{st} \text{ when } t = 0;\ \theta_p \text{ is the angular tooth pitch}),$$

$$g_j(\theta_j) = 1, \text{ when } \theta_{st} < \theta_j < \theta_{ex}, \text{ and } g_j(\theta_j) = 0, \text{ otherwise.}$$

θ_{st}, θ_{ex} are the start and exit immersion angles of the cutting range respectively.

The saw is modelled as an annular circular plate of inner radius a, outer radius b, and thickness h, rotating at a constant angular velocity Ω. The governing equation for transverse vibration in terms of the lateral displacement $w(r, \theta, t)$, with respect to space-fixed co-ordinates, can be written as

$$D\nabla^4 w + \rho h(w_{,tt} + 2\Omega w_{,t\theta} + \Omega^2 w_{,\theta\theta}) + L_s(w) = L_n(w) + f_c(t),$$

where D and ρ are the flexural rigidity and mass density of the plate respectively.

L_s is the membrane operator associated with the axisymmetric stress fields due to the centrifugal force and/or the stress tensioning. L_n is the membrane operator associated with the asymmetric stress fields generated by in-plane edge loads, such as in-plane cutting forces, which, under certain circumstances, may cause instability in such systems. In the present analysis, the effect of L_n will be neglected. $f_c(t)$ represents the transverse cutting forces generated by the interaction between the saw blade and the workpiece.

Substituting equation (1) into the equation of motion of the rotating disc and applying the Galerkin procedure leads to an equation of motion of the form

$$[M]\{\ddot{x}(t)\} + [G]\{\dot{x}(t)\} + [K]\{x(t)\} + (1 - e^{-TD})[A(t)]\{x(t)\} = \{0\}, \tag{2}$$

where e^{-TD} is a time delay operator (i.e., $e^{-TD}\{x(t)\} = \{x(t - T)\}$), and $[M]$, $[G]$ and $[K]$ represent the mass, gyroscopic and stiffness matrices, respectively, which may contain centrifugal stiffening and/or stress tensioning effects. The details of $[M]$, $[G]$, $[K]$ and $\{x\}$ are given in reference [9]. $[A(t)]$ is a periodic (T) time-varying matrix associated with the cutting forces.

The solution of equation (2) with periodic coefficients may be assumed in the form of a Fourier series with frequency components: $\lambda \pm ik\omega$ ($k = 0, 1, 2, \ldots$) ($\omega = 2\pi/T$; $i = \sqrt{-1}$) [16, 17].

$$\{x(t)\} = \left[\{b_0\}/2 + \sum_{k=1}^{\infty} (\{a_k\} \sin kwt + \{b_k\} \cos k\omega t)\right] e^{\lambda t}, \tag{3}$$

where $\{b_0\}$, $\{b_k\}$ and $\{a_k\}$ are time-invariant coefficient vectors; and λ is the characteristic variable of the system.

Since $[A(t)]$ is periodic, it can also be expressed in a Fourier series form as

$$[A(t)] = \frac{1}{2}[B_0] + \sum_{k=1}^{\infty} ([A_k] \sin k\omega t + [B_k] \cos k\omega t), \tag{4}$$

where

$$[B_0] = \frac{2}{T}\int_0^T [A(t)]\,\mathrm{d}t, \quad [B_k] = \frac{2}{T}\int_0^T [A(t)]\cos(k\omega t)\,\mathrm{d}t, \quad [A_k] = \frac{2}{T}\int_0^T [A(t)]\sin(k\omega t)\,\mathrm{d}t. \tag{5}$$

Substituting equations (3) and (4) into equation (2) and equating the coefficients of $e^{\lambda t}$, $e^{\lambda t}\sin k\omega t$ and $e^{\lambda t}\cos k\omega t$ to zero lead to the following form of the characteristic equation of the system:

$$(\lambda^2[H_2] + \lambda[H_1] + [H_0] + (1 - e^{-T\lambda})[L])\{s\} = \{0\}, \tag{6}$$

where $\{s\} = (\{b_0\}\ \{a_1\}\ \{b_1\} \cdots \{a_{N_s}\}\ \{b_{N_s}\})^{\mathrm{T}}$ and N_s is the number of components included in the Fourier series. The coefficient matrices $[H_2]$, $[H_1]$, $[H_0]$ and $[L]$ consist of $[K]$, $[G]$, $[M]$, $[B_0]$, $[B_k]$, $[A_k]$ and ω.

For the zeroth order approximation (i.e., $N_s = 0$), equation (2) can be written as

$$(\lambda^2[M] + \lambda[G] + [K] + (1 - e^{-T\lambda})[B_0]/2)\{b_0\} = \{0\}. \tag{7}$$

Appendix A contains a definition of the coefficient matrices of equation (6) for higher order approximations.

The single-mode solution for the blade deflection is assumed to be

$$w(r, \theta, t) = R_{mn}(r)[C_{mn}(t)\cos(n\theta) + S_{mn}(t)\sin(n\theta)], \tag{8}$$

where $R_{mn}(r)$ satisfies the plate boundary conditions corresponding to a clamped inner radius and a free outer radius.

Substituting equation (8) into the governing plate equation (without considering centrifugal stiffening or tensioning effects) and applying the Galerkin procedure leads to the equation

$$\begin{bmatrix} M_n & 0 \\ 0 & M_n \end{bmatrix} \begin{Bmatrix} \ddot{C}_{mn}(t) \\ \ddot{S}_{mn}(t) \end{Bmatrix} + \begin{bmatrix} 0 & 2\Omega n M_n \\ -2\Omega n M_n & 0 \end{bmatrix} \begin{Bmatrix} \dot{C}_{mn}(t) \\ \dot{S}_{mn}(t) \end{Bmatrix}$$

$$+ \begin{bmatrix} K_n - \Omega^2 n^2 M_n & 0 \\ 0 & K_n - \Omega^2 n^2 M_n \end{bmatrix} \begin{Bmatrix} C_{mn}(t) \\ S_{mn}(t) \end{Bmatrix} + (1 - e^{-TD})[A(t)] \begin{Bmatrix} C_{mn}(t) \\ S_{mn}(t) \end{Bmatrix} = \{0\}, \tag{9}$$

where

$$M_n = \rho h \pi \int_a^b R_{mn}^2(r) r\,\mathrm{d}r,$$

$$K_n = D\pi \left\{ \int_a^b \left[\left(\frac{\mathrm{d}}{\mathrm{d}r^2} + \frac{1}{r}\frac{\mathrm{d}}{\mathrm{d}r} - \frac{n^2}{r^2} \right)^2 R_{mn}(r) \right] R_{mn}(r) r\,\mathrm{d}r \right\}$$

and

$$[A(t)] = \sum_{j=1}^{N_t} g(\theta_j)[P(\theta_j)], \tag{10}$$

and where

$$[P(\theta_j)] = R_{mn}^2(r_0)\begin{bmatrix} K_r(\theta_j)\cos^2(n\theta_j) & K_r(\theta_j)\sin(2n\theta_j)/2 \\ K_r(\theta_j)\sin(2n\theta_j)/2 & K_r(\theta_j)\sin^2(n\theta_j) \end{bmatrix}.$$

$K_r(\theta_j)$ is a function of position θ_j for the case where the material of the workpiece is anisotropic. In the present case $K_r(\theta_j)$ is assumed constant.

The coefficient matrices $[B_0]$, $[B_k]$ and $[A_k]$ $(k = 1, 2, \dots)$ in equation (4) can be calculated efficiently by using the following scheme:

$$[B_0] = \frac{2}{T}\int_0^T [A(t)]\,\mathrm{d}t = \frac{2}{T}\int_0^T \sum_{j=1}^{N_t} g(\theta_j)[P(\theta_j)]\,\mathrm{d}t$$

$$= \frac{2}{T}\sum_{j=1}^{N_t}\int_{(j-1)T}^{jT} g(\tau)[P(\tau)]\,\mathrm{d}\tau = \frac{2}{\Omega T}\int_0^{N_t T\Omega} g(\theta)[P(\theta)]\,\mathrm{d}\theta.$$

Since $T = 2\pi/(N_t\Omega)$, $[B_0]$ can be rewritten as

$$[B_0] = \frac{N_t}{\pi}\int_0^{2\pi} g(\theta)[P(\theta)]\,\mathrm{d}\theta = \frac{N_t}{\pi}\int_{\theta_1}^{\theta_2} [P(\theta)]\,\mathrm{d}\theta. \tag{11}$$

Similarly,

$$[B_k] = \frac{N_t}{\pi}\int_{\theta_1}^{\theta_2} [P(\theta)]\cos(kN_t\theta)\,\mathrm{d}\theta, \quad [A_k] = \frac{N_t}{\pi}\int_{\theta_1}^{\theta_2} [P(\theta)]\sin(kN_t\theta)\,\mathrm{d}\theta. \tag{12, 13}$$

Substituting equations (11)–(13) into the characteristic equation (6) and employing *Müller's* optimization algorithm [18] to solve these complex non-linear equations yield the eigenvalues of the system.

In the case of multiple modes, the response at the location (r_0, θ_j) for a rotating circular saw subjected to regenerative cutting forces can be assumed to have the form

$$w(r_0, \theta_j, t) = \sum_{n=0}^{N}\sum_{m=0}^{M}\{R_{mn}(r_0)[C_{mn}(t)\cos(n\theta_j) + S_{mn}(t)\sin(n\theta_j)]\} \tag{14}$$

and the response of the blade at the previous cut $(t - T)$ at the same location can be expressed as

$$w(r_0, \theta_j, t - T) = \sum_{n=0}^{N}\sum_{m=0}^{M}\{R_{mn}(r_0)[C_{mn}(t - T)\cos(n\theta_j) + S_{mn}(t - T)\sin(n\theta_j)]\}, \tag{15}$$

where $S_{mn}(t)$ and $C_{mn}(t)$ can be assumed to have the same form as described in equation (3) with frequency components: $\lambda \pm \mathrm{i}k\omega$ $(k = 0, 1, 2, \dots, \omega = 2\pi/T)$.

Substituting equation (1) along with equations (14) and (15) into the governing equation and applying the Galerkin procedure result in the following equations:

$$\sum_{m=0}^{M}\alpha_l[\delta_{qml}^{(1)}\ddot{C}_{ml} + \delta_{qml}^{(2)}\dot{S}_{ml} + \delta_{qml}^{(3)}C_{ml}] + K_r(1 - \mathrm{e}^{-DT})\sum_{n=0}^{N}\sum_{m=0}^{M}[H_{mnql}^{(1)}C_{mn} + H_{mnql}^{(2)}S_{mn}] = 0, \tag{16}$$

$$-\sum_{m=0}^{M}\beta_l[\delta_{qml}^{(1)}\ddot{S}_{ml}-\delta_{qml}^{(2)}\dot{C}_{ml}+\delta_{qml}^{(3)}S_{ml}]+K_r(1-\mathrm{e}^{-DT})\sum_{n=0}^{N}\sum_{m=0}^{M}[H_{mnql}^{(3)}C_{mn}+H_{mnql}^{(4)}S_{mn}]=0,$$

$$(q=0,1,2,\ldots,M;\ l=0,1,2,\ldots,N), \tag{17}$$

where

$$H_{mnql}^{(1)}=\sum_{j=1}^{N_t}g(\theta_j)R_{mn}(r_0)R_{ql}(r_0)\cos(n\theta_j)\cos(l\theta_j),$$

$$H_{mnql}^{(2)}=\sum_{j=1}^{N_t}g(\theta_j)R_{mn}(r_0)R_{ql}(r_0)\sin(n\theta_j)\cos(l\theta_j),$$

$$H_{mnql}^{(3)}=\sum_{j=1}^{N_t}g(\theta_j)R_{mn}(r_0)R_{ql}(r_0)\cos(n\theta_j)\sin(l\theta_j),$$

$$H_{mnql}^{(4)}=\sum_{j=1}^{N_t}g(\theta_j)R_{mn}(r_0)R_{ql}(r_0)\sin(n\theta_j)\sin(l\theta_j),$$

and $\delta_{qml}^{(1)}$, $\delta_{qml}^{(2)}$ and $\delta_{qml}^{(3)}$ are given by

$$\delta_{qml}^{(1)}=\rho h\pi\int_a^b rR_{ml}(r)R_{ql}(r)\,\mathrm{d}r,\quad \delta_{qml}^{(2)}=\rho h\pi(2l\Omega)\int_a^b rR_{ml}(r)R_{ql}(r)\,\mathrm{d}r,$$

$$\delta_{qml}^{(3)}=D\pi\int_a^b r\{[\mathrm{d}^2/\mathrm{d}r^2+(1/r)\,\mathrm{d}/\mathrm{d}r-l^2]^2R_{ml}(r)\}R_{ql}(r)\,\mathrm{d}r$$

$$-h\pi\int_a^b\{(\mathrm{d}/\mathrm{d}r)[r\sigma_{rr}\mathrm{d}R_{ml}(r)/\mathrm{d}r]-(l^2/r)\sigma_{\theta\theta}R_{ml}(r)\}R_{ql}(r)\,\mathrm{d}r$$

$$-l^2\Omega^2\delta_{qml}^{(1)}.$$

$S_{mn}(t)$ and $C_{mn}(t)$ are then assumed to have form expressed by equation (3).

3. NUMERICAL RESULTS

In this section the results of numerical modelling, based upon the above developments, are presented and compared with experimental results.

Figure 3 shows the Campbell diagram (the variation of natural frequencies as measured by a stationary observer as a function of blade speed) and the variation of the real parts of the system eigenvalues as a function of speed for the (0, 2) mode of a rotating clamped circular saw-blade ($a=0{\cdot}08\,\mathrm{m}$, $b=0{\cdot}28\,\mathrm{m}$, $h=0{\cdot}0015\,\mathrm{m}$, $E=2{\cdot}08\mathrm{e}+11\,\mathrm{N/m^2}$, $\rho=7850\,\mathrm{kg/m^3}$, $v=0{\cdot}3$, $\theta_{st}=20^\circ$, $\theta_{ex}=50^\circ$, $N_t=40$). From this figure it is predicted that the primary instability region A (i.e., the widest region for which the real part of the eigenvalue is positive) occurs when the tooth-passing frequency $f_t=(\Omega/2\pi)N_t$ is greater than the natural frequency $f_n(\Omega)$ and less than twice this natural frequency, namely in the region $[f_n(\Omega), 2f_n(\Omega)]$ (note that the natural frequency f_n itself is also a function of rotation speed or tooth-passing frequency f_t). It may be noted that both the forward and the backward wave modes are unstable. This analysis was conducted using equation (7), i.e., using a zeroth order approximation. Further analyses using first and second order approximations gave essentially the same results.

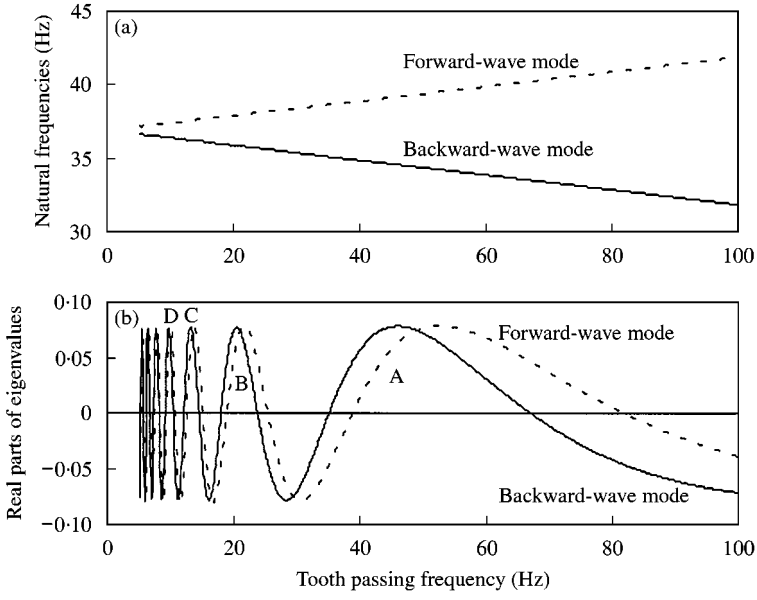

Figure 3. (a) Natural frequency and (b) instability regions of a rotating disc due to moving regenerative cutting forces; mode = (0, 2), $K_r = 10$ N/m; zeroth order approximation —— backward wave mode, – – – forward wave mode.

It was also found, from this Campbell diagram, that the rotating blade, subjected to regenerative cutting forces, also becomes unstable when

$$f_t = [\tfrac{1}{2} f_n(\Omega), \tfrac{2}{3} f_n(\Omega)] \quad \text{(Region } B\text{)},$$

$$f_t = [\tfrac{1}{3} f_n(\Omega), \tfrac{2}{5} f_n(\Omega)] \quad \text{(Region } C\text{)},$$

$$f_t = [\tfrac{1}{4} f_n(\Omega), \tfrac{2}{7} f_n(\Omega)] \quad \text{(Region } D\text{)},$$

$$\vdots$$

The general expression for unstable regions of a mode with natural frequency $f_n(\Omega)$ is given by

$$f_t = \left[\frac{1}{k} f_n(\Omega), \frac{1}{k - 0{\cdot}5} f_n(\Omega)\right] \quad (k = 1, 2, \dots). \tag{18}$$

From the simulations it was found that this expression is true for all modes. Thus, for each mode there are a number of different speed regions that will correspond to unstable behaviour. Which mode will result in washboarding depends upon the ability of the system to input more energy into that mode than is consumed by the energy dissipation mechanisms at work in that mode. In the experimental work, the primary region in which washboarding was excited corresponded to the widest instability region predicted, i.e., that region for which $f_t > f_n$. From these tests it was found that a number of different modes were excited at a given blade speed as would be expected from equation (18). The dominant mode was the one whose frequency was closest to the tooth-passing frequency. Note, however, from Figure 3 that as the tooth-passing frequency gets too close to the natural frequency the real part of the eigenvalue tends to zero and the response in that mode disappears. In the

present context, low-frequency modes are not excited because the saw cannot cut wood at slow speeds.

Cutting tests were conducted at different rotating speeds using clamped saw blades each with forty teeth, with inner radius $a = 0{\cdot}0952$ m, outer radius $b = 0{\cdot}265$ m and thickness $h = 0{\cdot}00229$ m; cutting two 36 mm deep Hemlock boards. The blades used were commercial blades that had been found to washboard in service. The blades were of uniform thickness with no holes or slots. The internal stress distribution was unknown.

In order to compare the experimental data with the stability predictions, the values of the natural frequencies of high order forward travelling modes are required. To this end, Figure 4 shows the Campbell diagram of a saw blade predicted from the measured natural frequencies of a stationary blade. In this prediction, the stiffening effect due to blade rotation has been neglected based upon the observation that, for the high-frequency modes excited by the washboarding the effect of rotational stiffening is small. On this diagram the line $f_t = f_n$ is superimposed.

According to equation (18), and considering the case $k = 1$, zones of unstable response for a mode with n nodal diameters could be expected at rotating speeds immediately above the crossing points denoted by $(0, nF)$. Figure 5 summarizes the results of experiments using the same blade. In Figure 5, the shaded region indicates those regions in which the washboarding was most pronounced. The individual points marked correspond to speeds at which low levels of washboarding were observed. It was found that the major washboarding zone lasted for a speed range of 100–150 r.p.m. As may be noted, the washboarding zones correspond to the unstable regions predicted by equation (18). The experimental results also provide qualitative confirmation of the analytical prediction that the magnitude of the real part of the eigenvalue is a maximum at a tooth passing frequency close to, but greater than the natural frequency of the dominant mode being excited.

Figure 6 compares the real parts of the eigenvalues for different K_r values. As may be noted, although the magnitudes of the real parts of the eigenvalues grow with the increase of K_r the instability regions remain almost unchanged for this set of K_r. A similar situation occurs when the number of active cutting teeth increases based on a change of the cutting

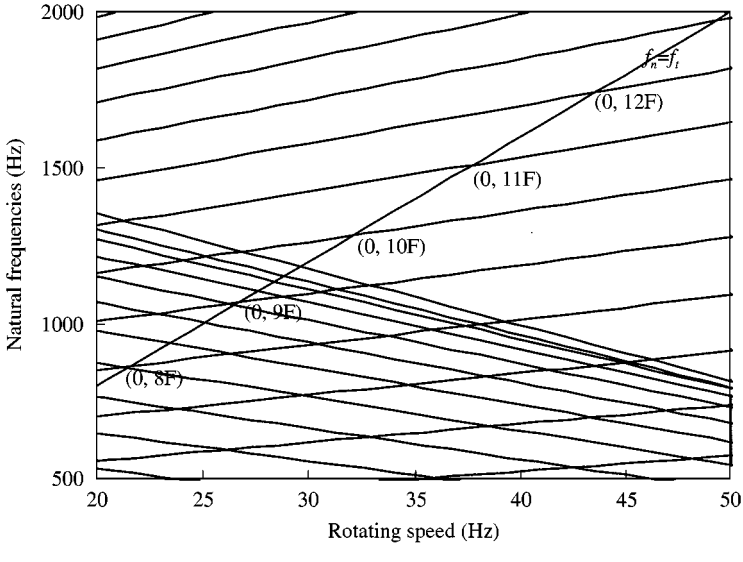

Figure 4. Campbell diagram predicted from the stationary natural frequencies.

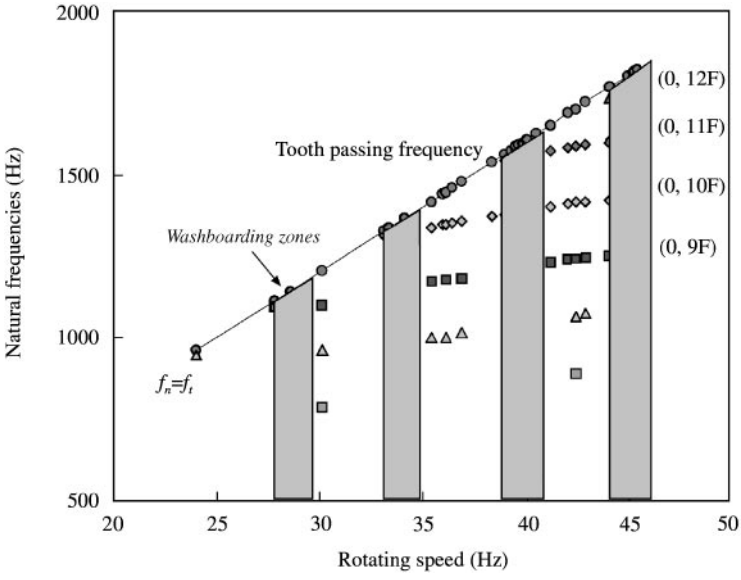

Figure 5. Rotational speeds at which washboarding was observed.

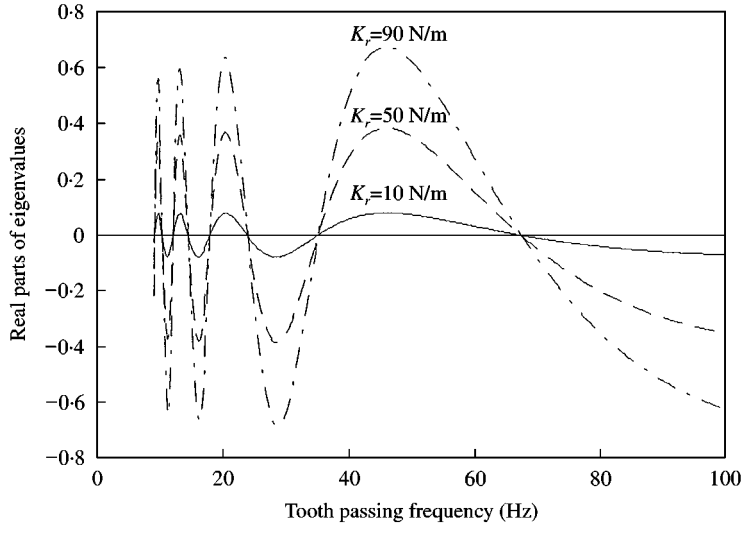

Figure 6. Effect of cutting coefficient K_r on instability regions of backward-wave mode (0, 2), zeroth order approximation (——, $K_r = 10$ N/m; – – –, $K_r =$ N/m; – – –, $K_r = 90$ N/m).

depth of the workpiece, as shown in Figure 7. These results correspond to experimental observations that the intensity of washboarding is increased with increasing wood density (increasing K_r), and with increasing depth of cut.

Figure 8 shows a two-mode solution for the rotating circular saw blade which has the same geometry as that used for the results shown in Figure 3. As may be noted, the results related to each mode in the two-mode solution are very similar to the ones from the single-mode solution and no coupling instability regions are found at subcritical speeds. This figure also reveals that the real parts of the eigenvalues in mode (0, 5) are greater than

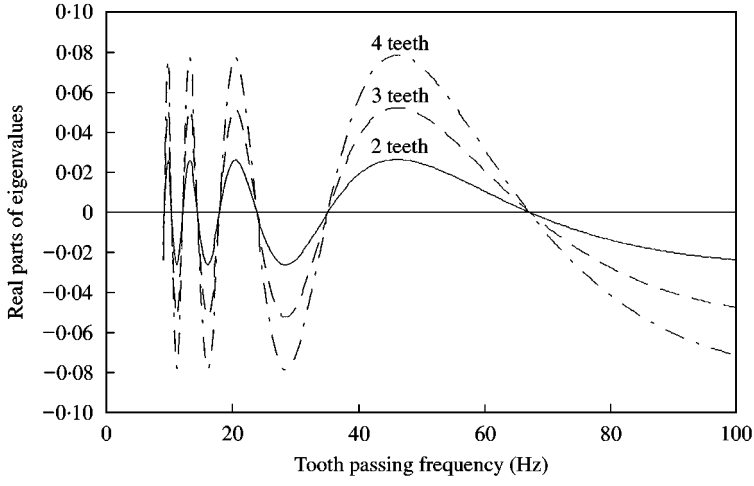

Figure 7. Effect of different numbers of active cutting teeth on instability regions of backward-wave mode (0, 2); zeroth order approximation; $K_r = 10$ N/m (——, 2 teeth; – – –, 3 teeth; – – –, 4 teeth).

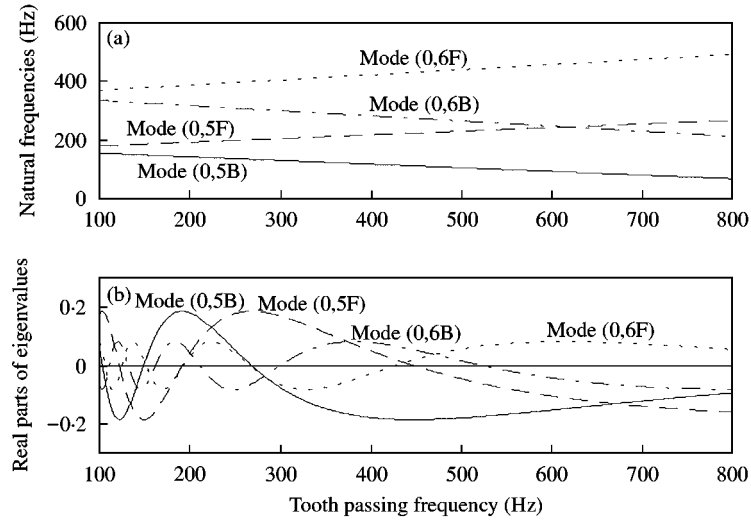

Figure 8. (a) Natural frequency and (b) instability regions caused by moving regenerative cutting forces on modes (0, 5) and (0, 6); $K_r = 100$ N/m; zeroth order approximation (——, mode (0, 5B); – – –, mode (0, 5F); – – –, mode (0, 6B); - - -, mode (0, 6F)).

the ones in mode (0, 6). From numerous stability simulations in saw-blade cutting and metal cutting conducted as part of this research work, it was found that the levels of the real parts of the eigenvalues for different modes are associated with the magnitude of the modal displacements of the stationary blade at the cutting points. This implies, in this idealized model, that the displacements contributed by mode (0, 5) were greater than those from mode (0, 6).

Figure 9 shows a two-mode Campbell diagram that extends into the supercritical speed range. From this figure it can be seen that, in such a system, both the backward-wave modes become unstable at supercritical speeds.

Figure 9 also illustrates that several modes of the blade can be excited simultaneously and different number of vibration modes may be excited at different tooth-passing frequencies

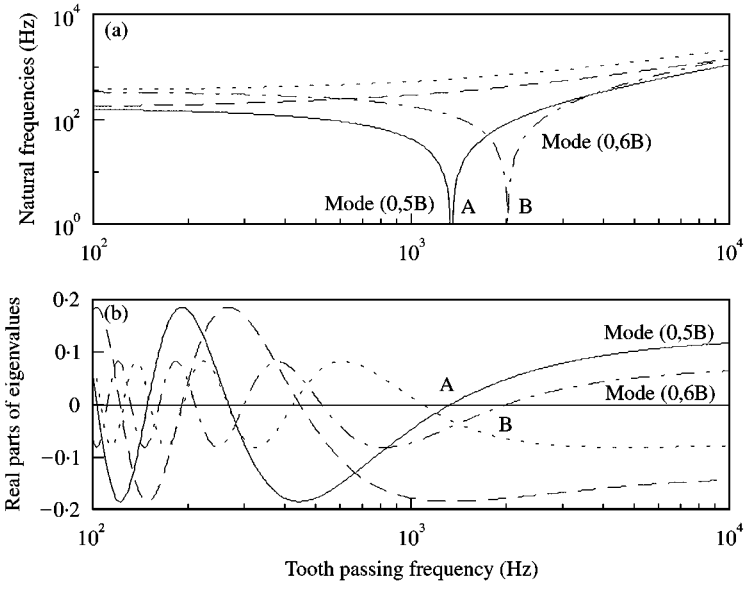

Figure 9. (a) Natural frequency and (b) instability regions at subcritical and supercritical blade speeds for modes (0, 5) and (0, 6); $K_r = 100$ N/m; zeroth order approximation (——, mode (0, 5B); – – –, mode (0, 5F); – · –, mode (0, 6B); - - -, mode (0, 6F)).

(or rotating speeds). It should be mentioned that in saw-blade cutting the levels of the self-excited vibration of the blade during cutting is not only related to its stability characteristics (i.e., the real parts of the eigenvalues of the system) but are also associated with its initial vibration conditions.

4. KINEMATICS OF WASHBOARDING

The above analysis predicts speed ranges at which unstable blade response can be expected based upon the linear undamped plate model used in this study. In order to predict the actual displacements would require an analysis that accounted for the geometric non-linear behaviour of the saw, the energy dissipation mechanisms, and a more detailed cutting force model. Such a task is beyond the scope of the present study. Instead a simple kinematic analysis of the actual response of the blade as it passes through the wood is presented and shown to be consistent with experimental results.

Figure 10 shows the positions of the teeth at the previous and current cuts. It can be assumed that tooth A reaches its maximum lateral displacement A_0 at $t = 0$ when this tooth enters the wood. The lateral response of the blade at a point stationary in space can thus be expressed in the form $w = A_0 \cos(2\pi f_n t)$ (where f_n is the resonant frequency of the blade), based on the assumption that only one mode is excited. The next tooth (i.e., tooth B) will take $1/f_t$ of time to reach the same vertical position. At this point in time, the blade vibrates laterally to a location where $w_1 = A_0 \cos(2\pi f_n \Delta T)$. From Figure 11 it is clear that

$$\Delta T = 1/f_n - 1/f_t \tag{19}$$

for the case that $2f_n > f_t > f_n$.

It is assumed that there are N teeth passing through the same horizontal line CD in the time period dt (dt must be such that N is an integer). Thus, the lateral displacement of the

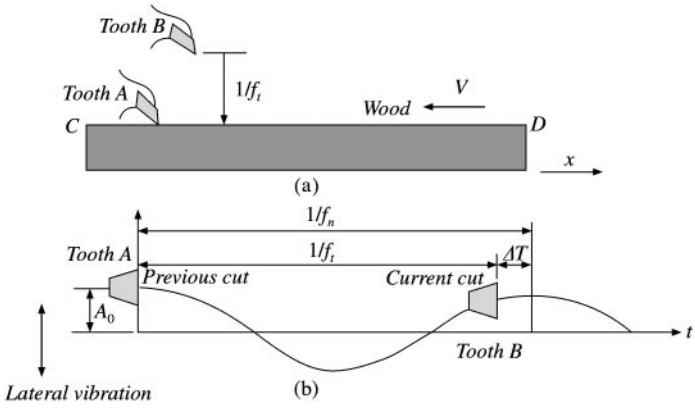

Figure 10. Tooth kinematics during cutting. (a) side view at $t = 0$; (b) plan view of tooth motion over one complete cycle.

Nth tooth can be expressed in the time domain as

$$w_N = A_0 \cos(2\pi f_n N \Delta T) \quad (N = 1, 2, \ldots), \tag{20}$$

where $N = f_t \, \mathrm{d}t$ and $\mathrm{d}t = x/V$ (where V is the feed speed of the wood).

Substituting equation (19) and the above expressions for N and $\mathrm{d}t$ into equation (20) results in a lateral displacement $w(x)$ in the space domain x, where

$$w(x) = A_0 \cos\left(2\pi \frac{f_t - f_n}{V} x\right) = A_0 \cos\left(2\pi \frac{1}{\lambda_x} x\right), \tag{21}$$

which is also the pattern produced by the teeth of the blade along an arbitrary horizontal line on the cut surface. Thus, the wavelength of the washboarding pattern can be written as

$$\lambda_x = \frac{V}{f_t - f_n}. \tag{22}$$

Note that equation (22) is derived based on the assumption that the response of the blade is purely harmonic. From this equation, it can be seen that the wavelength λ_x is proportional to the feed speed of the workpiece V and is inversely proportional to the difference between the tooth-passing frequency f_t and the resonant frequency of the blade f_n.

A comparison was made of the washboarding patterns produced by the saw-blade with approximately equal feed speeds of the workpiece ($V = 0{\cdot}84$ m/s) but different $\Delta f = f_t - f_n$. The differences between f_t and f_n were $\Delta f = 36{\cdot}7$ Hz for case (a) and $\Delta f = 59{\cdot}8$ Hz for case (b). Thus, the washboarding wavelengths can be predicted from equation (22), and give the values $\lambda_x = 22{\cdot}8$ mm for case (a) and $\lambda_x = 14{\cdot}0$ mm for case (b), which agree well with the measured wavelengths: $\lambda_x = 21{\cdot}8$ mm to $22{\cdot}3$ mm for case (a) and $\lambda_x = 13{\cdot}0$ mm to $13{\cdot}4$ mm for case (b).

5. SUMMARY

An analysis of the stability characteristics of a rotating disc subjected to discrete regenerative moving forces applied over a space-fixed sector of the disc rim has been presented. This analysis shows that there is a number of distinct speed regions over which

unstable vibration behaviour is predicted. The largest unstable region is associated with the case where the force excitation frequency was somewhat greater than the natural frequency of the mode being excited. This model was applied to the analysis of a vibration instability known as washboarding that occurs in wood cutting circular saws and was shown to produce accurate simulations of the behaviour of the saw.

ACKNOWLEDGMENT

Funds for this study were provided by the National Science and Engineering Research Council of Canada.

REFERENCES

1. J. TIAN 1998 *Ph.D. Thesis, Department of Mechanical Engineering. The University of British Columbia, Vancouver, B.C., Canada.* Self excited vibration of rotating discs and shafts with applications to sawing and milling.
2. J. F. CARLIN, F. C. APPL, H. C. BRIDWELL and R. P. DUBIOS 1975 ASME *Journal of Engineering for Industry, Series B* **97**, 37–48. Effects of tension on buckling and vibration of circular saw blades.
3. C. J. RADCLIFFE and C. D. MOTE JR 1977 *International Journal of Mechanical Science* **19**, 567–574. Stability of stationary and rotating discs under edge load.
4. J. S. CHEN and D. B. BOGY 1993 ASME *Journal of Applied Mechanics* **60**, 646–648. The effects of a space-fixed friction force on the in-plane stress and stability of transverse vibrations of a spinning disk.
5. S. CHONAN, Z. W. JIANG and Y. YUKI 1993 ASME *Journal of Vibration and Acoustics* **114**, 529–534. Vibration and deflection of a silicon-wafer slicer cutting the crystal ingot.
6. J. S. CHEN 1994 ASME *Journal of Applied Mechanics* **61**, 788–792. Stability analysis of a spinning elastic disk under a stationary concentrated edge load.
7. I. Y. SHEN and Y. SONG 1996 ASME *Journal of Applied Mechanics* **63**, 121–127. Stability and vibration of a rotating circular plate subjected to stationary in-plane edge loads.
8. J. S. CHEN 1997 ASME *Journal of Applied Mechanics* **64**, 139–143. Parametric response of a spinning disk under space-fixed pulsating edge loads.
9. J. TIAN and S. G. HUTTON 1999 ASME *Journal of Applied Mechanics* **66**, 800–805. Self-excitation in flexible rotating discs subjected to various transverse interactive forces—a general approach.
10. S. A. TOBIAS 1965 *Machine Tool Vibration.* New York: Wiley.
11. H. E. MERRITT 1965 ASME *Journal of Engineering for Industry* **87**, 447–454. Theory of self-excited machine tool chatter.
12. J. TLUSTY and F. ISMAIL 1983 ASME *Journal of Vibration, Stress and Reliability in Design* **105**, 24–32. Special aspects of chatter in milling.
13. I. MINIS and T. YANUSHEVSKY 1993 ASME *Journal of Engineering for Industry* **115**, 1–8. A new theoretical approach for the prediction of machine tool chatter.
14. Y. ALTINTAS and E. BUDAK 1995 *Annals of the CIRP* **44**, 357–362. Analytical prediction of stability lobes in milling.
15. J. TIAN and S. G. HUTTON 1999 *Journal of Manufacturing Science and Engineering.* Chatter instability in milling systems with flexible rotating spindles—a new theoretical approach. (in press).
16. V. V. BOTLTIN 1964 *The Dynamic Stability of Elastic Systems.* San Francisco: Holden-Day.
17. L. LENGOC 1995 *Journal of Sound and Vibration* **186**, 143–162. Wide bandsaw blade under cutting condition, Part II: stability of a plate moving in its plane while subjected to parametric excitation.
18. J. H. MATHEWS 1992 *Numerical Methods for Mathematics, Science and Engineering.* Englewood Cliffs, NJ: Prentice-Hall Inc. second edition.

APPENDIX A: COEFFICIENT MATRICES

The characteristic equation of the system is given by

$$(\lambda^2[H_2] + \lambda[H_1] + [H_0] + (1 - e^{-T\lambda})[L])\{s\} = \{0\}. \tag{A1}$$

For the first order approximation (i.e., $N_s = 1$), $[H_2]$, $[H_1]$, $[H_0]$ and $[L]$ are (for the sake of simplicity of expression, let $\mathbf{M} = [M]$, $\mathbf{G} = [G]$, $\mathbf{K} = [K]$,

$$[H_2] = \begin{bmatrix} \frac{1}{2}\mathbf{M} & \mathbf{0} & \mathbf{0} \\ \mathbf{0} & \mathbf{M} & \mathbf{0} \\ \mathbf{0} & \mathbf{0} & \mathbf{M} \end{bmatrix}, \quad [H_1] = \begin{bmatrix} \frac{1}{2}\mathbf{G} & \mathbf{0} & \mathbf{0} \\ \mathbf{0} & \mathbf{G} & -2\omega\mathbf{M} \\ \mathbf{0} & 2\omega\mathbf{M} & \mathbf{G} \end{bmatrix},$$

$$[H_0] = \begin{bmatrix} \frac{1}{2}\mathbf{K} & \mathbf{0} & \mathbf{0} \\ \mathbf{0} & \mathbf{K} - \omega^2\mathbf{M} & -\omega\mathbf{G} \\ \mathbf{0} & \omega\mathbf{G} & \mathbf{K} - \omega^2\mathbf{M} \end{bmatrix}, \quad [L] = \begin{bmatrix} \frac{1}{4}\mathbf{B}_0 & \frac{1}{2}\mathbf{A}_1 & \frac{1}{2}\mathbf{B}_1 \\ \frac{1}{2}\mathbf{A}_1 & \frac{1}{2}(\mathbf{B}_0 - \mathbf{B}_2) & \frac{1}{2}\mathbf{A}_2 \\ \frac{1}{2}\mathbf{B}_1 & \frac{1}{2}\mathbf{A}_2 & \frac{1}{2}(\mathbf{B}_0 + \mathbf{B}_2) \end{bmatrix},$$

$$\{s\} = (\{b_0\}\ \{a_1\}\ \{b_1\})^{\mathrm{T}}.$$

For a general case (i.e., the N_sth order approximation), the coefficient matrices in the characteristic equation can be written as

$$[H_2] = \begin{bmatrix} \frac{1}{2}\mathbf{M} & & & & \\ & \mathbf{M} & & \mathbf{0} & \\ & & \mathbf{M} & & \\ & & & \ddots & \\ & \mathbf{0} & & \mathbf{M} & \\ & & & & \mathbf{M} \end{bmatrix},$$

$$[H_1] = \begin{bmatrix} \frac{1}{2}\mathbf{G} & & & & & \\ & \mathbf{G} & -2\omega\mathbf{M} & & \mathbf{0} & \\ & 2\omega\mathbf{M} & \mathbf{G} & & & \\ & & & \ddots & & \\ & \mathbf{0} & & & \mathbf{G} & -2N_s\omega\mathbf{M} \\ & & & & 2N_s\omega\mathbf{M} & \mathbf{G} \end{bmatrix},$$

$$[H_0] = \begin{bmatrix} \frac{1}{2}\mathbf{K} & & & & & \\ & \mathbf{K} - \omega^2\mathbf{M} & -\omega\mathbf{G} & & \mathbf{0} & \\ & \omega\mathbf{G} & \mathbf{K} - \omega^2\mathbf{M} & & & \\ & & & \ddots & & \\ & \mathbf{0} & & & \mathbf{K} - N_s^2\omega^2\mathbf{M} & -N_s\omega\mathbf{G} \\ & & & & N_2\omega\mathbf{G} & \mathbf{K} - N_s^2\omega^2\mathbf{M} \end{bmatrix},$$

$$[L] = \begin{bmatrix} \frac{1}{4}\mathbf{B}_0 & \frac{1}{2}\mathbf{A}_1 & \frac{1}{2}\mathbf{B}_1 & \cdots & \cdots & \frac{1}{2}\mathbf{A}_{N_s} & \frac{1}{2}\mathbf{B}_{N_s} \\ \frac{1}{2}\mathbf{A}_1 & \frac{1}{2}(\mathbf{B}_0 - \mathbf{B}_2) & \frac{1}{2}\mathbf{A}_2 & & & \vdots & \vdots \\ \frac{1}{2}\mathbf{B}_1 & \frac{1}{2}\mathbf{A}_2 & \frac{1}{2}(\mathbf{B}_0 + \mathbf{B}_2) & & & \frac{1}{2}(\mathbf{B}_l - \mathbf{B}_{2N_s-l}) & \frac{1}{2}(-\mathbf{A}_l + \mathbf{A}_{2N_s-l}) \\ \vdots & & & \ddots & & \frac{1}{2}(\mathbf{A}_l + \mathbf{A}_{2N_s-l}) & \frac{1}{2}(\mathbf{B}_l + \mathbf{B}_{2N_s-l}) \\ \vdots & & & & \ddots & \vdots & \vdots \\ \frac{1}{2}\mathbf{A}_{N_s} & \cdots & \frac{1}{2}(\mathbf{B}_l - \mathbf{B}_{2N_s-l}) & \frac{1}{2}(\mathbf{A}_l + \mathbf{A}_{2N_s-l}) & \cdots & \frac{1}{2}(\mathbf{B}_0 - \mathbf{B}_{2N_s}) & \frac{1}{2}\mathbf{A}_{2N_s} \\ \frac{1}{2}\mathbf{B}_{N_s} & \cdots & \frac{1}{2}(-\mathbf{A}_l + \mathbf{A}_{2N_s-l}) & \frac{1}{2}(\mathbf{B}_l + \mathbf{B}_{2N_s-l}) & \cdots & \frac{1}{2}\mathbf{A}_{2N_s} & \frac{1}{2}(\mathbf{B}_0 + \mathbf{B}_{2N_s}) \end{bmatrix},$$

$$\{s\} = (\{b_0\}\ \{a_1\}\ \{b_1\}\ \cdots\ \{a_{N_s}\}\ \{b_{N_s}\})^{\mathrm{T}},$$

where the general expression of diagonal sub-matrices in $[L]$ can be written as

$$\begin{bmatrix} \frac{1}{2}(\mathbf{B}_0 - \mathbf{B}_{2N_s}) & \frac{1}{2}\mathbf{A}_{2N_s} \\ \frac{1}{2}\mathbf{A}_{2N_s} & \frac{1}{2}(\mathbf{B}_0 + \mathbf{B}_{2N_s}) \end{bmatrix}$$

and the non-diagonal sub-matrices above the diagonal sub-matrix shown above can be expressed in the form

$$\begin{bmatrix} \frac{1}{2}(\mathbf{B}_{0+l} - \mathbf{B}_{2N_s-l}) & \frac{1}{2}(-\mathbf{A}_{0+l} + \mathbf{A}_{2N_s-l}) \\ \frac{1}{2}(\mathbf{A}_{0+l} + \mathbf{A}_{2N_s-l}) & \frac{1}{2}(\mathbf{B}_{0+l} + \mathbf{B}_{2N_s-l}) \end{bmatrix} \quad (l = 1, 2, \ldots, N_s - 1),$$

where l is the number of sub-matrix rows counting from the diagonal sub-matrix up to the second row sub-matrix.

As an example of $[L]$ when $N_s = 3$, the following matrix is obtained:

$$\begin{bmatrix} \frac{1}{4}\mathbf{B}_0 & \frac{1}{2}\mathbf{A}_1 & \frac{1}{2}\mathbf{B}_1 & \frac{1}{2}\mathbf{A}_2 & \frac{1}{2}\mathbf{B}_2 & \frac{1}{2}\mathbf{A}_3 & \frac{1}{2}\mathbf{B}_3 \\ \frac{1}{2}\mathbf{A}_1 & \frac{1}{2}(\mathbf{B}_0 - \mathbf{B}_2) & \frac{1}{2}\mathbf{A}_2 & \frac{1}{2}(\mathbf{B}_1 - \mathbf{B}_3) & \frac{1}{2}(-\mathbf{A}_1 + \mathbf{A}_3) & \frac{1}{2}(\mathbf{B}_2 - \mathbf{B}_4) & \frac{1}{2}(-\mathbf{A}_2 + \mathbf{A}_4) \\ \frac{1}{2}\mathbf{B}_1 & \frac{1}{2}\mathbf{A}_2 & \frac{1}{2}(\mathbf{B}_0 + \mathbf{B}_2) & \frac{1}{2}(\mathbf{A}_1 + \mathbf{A}_3) & \frac{1}{2}(\mathbf{B}_1 + \mathbf{B}_3) & \frac{1}{2}(\mathbf{A}_2 + \mathbf{A}_4) & \frac{1}{2}(\mathbf{B}_2 + \mathbf{B}_4) \\ \frac{1}{2}\mathbf{A}_2 & \frac{1}{2}(\mathbf{B}_1 - \mathbf{B}_3) & \frac{1}{2}(\mathbf{A}_1 + \mathbf{A}_3) & \frac{1}{2}(\mathbf{B}_0 - \mathbf{B}_4) & \frac{1}{2}\mathbf{A}_4 & \frac{1}{2}(\mathbf{B}_1 - \mathbf{B}_5) & \frac{1}{2}(-\mathbf{A}_1 + \mathbf{A}_5) \\ \frac{1}{2}\mathbf{B}_2 & \frac{1}{2}(-\mathbf{A}_1 + \mathbf{A}_3) & \frac{1}{2}(\mathbf{B}_1 + \mathbf{B}_3) & \frac{1}{2}\mathbf{A}_4 & \frac{1}{2}(\mathbf{B}_0 + \mathbf{B}_4) & \frac{1}{2}(\mathbf{A}_1 + \mathbf{A}_5) & \frac{1}{2}(\mathbf{B}_1 + \mathbf{B}_5) \\ \frac{1}{2}\mathbf{A}_3 & \frac{1}{2}(\mathbf{B}_2 - \mathbf{B}_4) & \frac{1}{2}(\mathbf{A}_2 + \mathbf{A}_4) & \frac{1}{2}(\mathbf{B}_1 - \mathbf{B}_5) & \frac{1}{2}(\mathbf{A}_1 + \mathbf{A}_5) & \frac{1}{2}(\mathbf{B}_0 - \mathbf{B}_6) & \frac{1}{2}\mathbf{A}_6 \\ \frac{1}{2}\mathbf{B}_3 & \frac{1}{2}(-\mathbf{A}_2 + \mathbf{A}_4) & \frac{1}{2}(\mathbf{B}_2 + \mathbf{B}_4) & \frac{1}{2}(-\mathbf{A}_1 + \mathbf{A}_5) & \frac{1}{2}(\mathbf{B}_1 + \mathbf{B}_5) & \frac{1}{2}\mathbf{A}_6 & \frac{1}{2}(\mathbf{B}_0 + \mathbf{B}_6) \end{bmatrix}.$$

Müller's algorithm with deflation for solving non-linear equations [18] is employed to find the roots of equation (A1).